A Numerical Study of Shock Reflection Phenomena in Shock/Turbulence Interaction

MOHAMMAD ALI JINNAH
Department of Mechanical and Chemical Engineering
Islamic University of Technology (IUT)
Board Bazar, Gazipur-1704
BANGLADESH

Abstract: - Shock reflection phenomena have been studied numerically in shock/turbulence interaction where different types of shock reflector are used for the partial reflection of the shock wave. The three-dimensional Reynolds-averaged Navier-stokes equations with k-ε turbulence model are solved and the results have been compared with the Navier-Stokes Simulation (NS) results. The comparisons indicate that the present turbulence model is working very well in shock reflection phenomena for the reflection from different shock reflectors. Different strengths of reflected shock wave after reflection from the shock reflectors of 49.0 % opening area, 26.5 % opening area and from the plane end wall interact with the same turbulence field. The outcomes of shock/turbulence interaction are highly influenced by the strength of the reflected shock wave and the longitudinal velocity across the shock wave. The longitudinal velocity behind the reflected shock wave increases due to the partial reflection from the shock reflectors and the higher longitudinal velocities are obtained in the downstream of the reflected shock wave after reflection from the shock reflector of higher openings. In the case of partial reflection, the static temperature deviations are observed in the downstream region and the deviations are higher for the interaction of stronger reflected shock wave. The turbulent length scales are measured in the upstream and downstream of the reflected shock wave and it is observed that the amplification of the turbulent length scales decrease after the shock/turbulence interaction. The rate of dissipation of turbulent kinetic energy decreases after the interaction of different strengths of shock wave with turbulent field.

Key-Words: - Shock wave, Turbulent flow, Navier-Stokes equations, Turbulence model

1 Introduction

The study of shock reflection phenomena is the important part in shock/turbulence interaction. Many researchers were used the plane end wall of the shock tube for the reflected shock wave and the reflected shock wave later was used to interact with the shock-induced turbulent flow. In the present study, special types of shock reflector are used for the different strengths of reflected shock wave to interact in the turbulent field. The incident shock after passing through turbulence-generating grids becomes distorted and converges again to become a plane shock wave. Due to shock wave distortion, a homogenous turbulent field is appeared after a certain distance in the wake of the turbulence grids. The transmitted shock wave, which is weaker than the incident shock wave, reflects from the shock reflector and start moving through the turbulent field in the upstream of the reflected shock wave. The strength of the reflected shock wave depends on the open area ratio of the shock reflector. Due to partial reflection from the shock reflector, both deflection and distortion are appeared in the reflected shock wave at the initial stage of the reflection and after traveling a short distance; the non-plane reflected shock wave converges to form again the plane normal shock wave and interacts with the grid-generated turbulent field. The reflected shock wave strength is measured numerically for the shock reflector of 26.5% openings and 49.5% openings and for the plane end wall. The fully reflected shock wave is observed from the plane end wall and in the case of the full reflection; the longitudinal velocity in the downstream of the reflected shock wave is nearly zero. So using the shock reflector is the advantage of the increasing the longitudinal velocity in the downstream of the reflected shock wave. Due to increasing the longitudinal velocity behind the reflected shock wave, it is possible to avoid the non-flow turbulent field after the shock wave interaction. Different longitudinal velocities are obtained for the reflection from the shock reflector

of different openings and the non-flow turbulent field is obtained after the interaction of shock wave reflected from the plane end wall. A. Honkan and J. Andreopoulos [1] used Rigimesh disk instead of the end wall to obtain a nonzero velocity flow field behind the reflected shock wave and it is one of the full reflection cases even though Rigimesh disk is used instead of the end wall. They used hot wire techniques to measure the turbulence intensity at different locations. J. Keller and W. Merzkirch [2] conducted experiments on the grid-generated turbulent field, interact with the reflected shock wave. In this experimental work, the position of the reflected shock wave adjusted by changing the position of the shock tube's end wall and the reflected shock wave interacted with the grid-generated turbulence. Many researchers were used turbulence grid to generate turbulent field in the wake of the grid plate due to the shock wave diffraction. The elementary waves formed by diffraction of the wave at the grid propagate in downstream direction and after a short period converge to form again plane, normal shock which is weaker than the incident shock wave. The plane shock after reflection from the end wall of the tube interacts with the grid-generated turbulent field. In the present computation, a shock reflector is used instead of end wall to study special shock reflection phenomena numerically. The study of such types of reflection phenomena enhances the investigation on shock/turbulence interaction properly. Experimental realization of a homogeneous and isotropic turbulent flow interacting with a normal shock wave in the laboratory is a difficult task due to generation of compressible and isotropic turbulent flow and the generation of a normal shock wave interacting with flow. Experimentally and numerically many researchers got many results on shock/turbulence interaction. The outcomes of the interactions of shock wave with homogeneous and isotropic turbulence are the amplification of longitudinal velocity fluctuations, the amplification of turbulent kinetic energy level and substantial changes in length scales. Debreve and Lacharme [3] conducted experiments on the interaction between the shock wave and the grid-generated turbulence and they measured velocity and temperature spectra upstream and downstream of the shock wave and concluded that turbulent fluctuations are amplified and Taylor micro scales increase during the interaction. Jacquin, Blin and Gaffray [4] investigated the interactions of a normal shock wave with grid-generated turbulence and a turbulent jet and they observed that turbulence amplification was not significant for the grid-generated turbulence and that the decay of turbulent kinetic energy was accelerated downstream of the shock wave. Their experiments treated the interaction of a shock with quasi-incompressible turbulence where fluctuations in pressure and density are not significant. An experiment on the interaction of weak shocks (M_s=1.007, 1.03 and 1.1) with a random medium of density in homogeneity was performed by Hesselink and Sturtevant [5]. They observed that the pressure histories of the distorted shock waves were both peaked and rounded and explained these features in terms of the focusing/defocusing of the shock front due to in homogeneity of the medium.

Numerical techniques for such types of interactions are more suitable to get the reliable results and easily estimate the physical data structure, which can difficult to measure in experiment. Using a shock capturing numerical technique, Rotman [6] numerically calculated the change in a two-dimensional turbulent flow caused by the passage of a traveling shock wave. He found that the shock causes in increase in the turbulent kinetic energy and that the length scale of the turbulent field is reduced upon passage of the shock. He also found that increasing the initial turbulent kinetic energy caused a straight shock wave to evolve into a distorted front. Lee, Lele and Moin [7] conducted direct numerical simulations of two-dimensional turbulence interacting with a shock wave and found that vorticity amplification compared well with the predictions of the linear analysis but turbulent kinetic energy evolution behind the shock showed significant nonlinear effects. The energy spectrum was found to be enhanced more at large wave numbers, leading to an overall length scale decrease. It is observed from all previous research works on shock/turbulence interaction that most of the interaction works are performed by the shock wave, reflected from the plane end wall and the longitudinal velocity in the downstream of the reflected shock wave is very low. But in the present computational works, the shock reflectors are used to change the strength of the reflected shock wave and to change the longitudinal velocity across the reflected shock. For the present numerical simulation, the three-dimensional Navier-stokes equations using k-ε turbulence model are solved to study the shock reflection phenomena by shock capturing method where for more accurate solutions, the grid adaptation technique is used. Grid adaptation technique with k-ε turbulence model are the improve technique for numerical simulation of shock/turbulence interaction.

2 Numerical Methods

2.1 Governing equations

The three-dimensional unsteady, compressible, Reynolds-averaged Navier-stokes equations with k-ε turbulence model are solved by shock capturing method. Without external forces and heat sources, the conservative form of non-dimensionalized governing equation in three-dimensional Cartesian coordinate system is,

$$\frac{\partial Q}{\partial t}+\frac{\partial (F-Fv)}{\partial x}+\frac{\partial (G-Gv)}{\partial y}+\frac{\partial (H-Hv)}{\partial z}=S(Q)$$

where, $Q = [\rho, \rho u, \rho v, \rho w, e, \rho k, \rho \varepsilon]$,
$F = [\rho u, \rho u^2, \rho uv, \rho uw, u(e+p)\ , \rho uk, \rho u\varepsilon]$,
$G = [\rho v, \rho uv, \rho v^2, \rho vw, v(e+p)\ , \rho vk, \rho v\varepsilon]$,
$H = [\rho w, \rho uw, \rho vw, \rho w^2, w(e+p)\ , \rho wk, \rho w\varepsilon]$ and
$Fv = [0, \tau_{xx}, \tau_{xy}, \tau_{xz}, u\tau_{xx}+v\tau_{xy}+w\tau_{xz}-q_x, k_x, \varepsilon_x]$,
$Gv = [0, \tau_{xy}, \tau_{yy}, \tau_{yz}, u\tau_{xy}+v\tau_{yy}+w\tau_{yz}-q_y, k_y, \varepsilon_y]$,
$Hv = [0, \tau_{xz}, \tau_{yz}, \tau_{zz}, u\tau_{xz}+v\tau_{yz}+w\tau_{zz}-q_z\ , k_z, \varepsilon_z]$

Here Q is the vector of conservative variables which contain mass, momentum and energy. All variables are calculated in per unit volume. Three momentum terms in three-dimensional Cartesian coordinates system are ρu, ρv and ρw per unit volume. Total energy, e, turbulent kinetic energy, ρk and turbulent dissipative energy, $\rho\varepsilon$ are the energy terms per unit volume. F, G and H are the three inviscid flux vectors in X-, Y-, and Z-axis respectively. Similarly F_v, G_v and H_v are the three viscous flux vectors in X-, Y-, and Z-axis respectively. Each flux vectors contain mass flux, momentum flux and energy flux. ρu is the mass flux and ρu^2, ρuv, ρuw are the momentum flux and $u(e+p)$, ρuk, $\rho u\varepsilon$ are the energy flux in the X-axis. Similarly ρv is the mass flux and ρuv, ρv^2, ρvw are the momentum flux and $v(e+p)$, ρvk, $\rho v\varepsilon$ are the energy flux in the Y-axis. ρw is the mass flux and ρwu, ρvw, ρw^2 are the momentum flux and $w(e+p)$, ρwk, $\rho w\varepsilon$ are the energy flux in the Z-axis. Also ρ is the fluid density and u, v and w are velocity components in each direction of Cartesian coordinates. While e is the total energy per unit volume, pressure p can be expressed by the following state equation for ideal gas:

$$p = (\gamma -1)[e-\tfrac{1}{2}\rho(u^2+v^2+w^2)]$$

where γ is the ratio of specific heats.

From the relationship between stress and strain and assumption of stokes, non-dimensional stress components are as follows

$$\tau_{xx}=\frac{\mu}{\mathrm{Re}}\tfrac{2}{3}\left(2.\frac{\partial u}{\partial x}-\frac{\partial v}{\partial y}-\frac{\partial w}{\partial z}\right),$$

$$\tau_{yy}=\frac{\mu}{\mathrm{Re}}\tfrac{2}{3}\left(2.\frac{\partial v}{\partial y}-\frac{\partial w}{\partial z}-\frac{\partial u}{\partial x}\right),$$

$$\tau_{zz}=\frac{\mu}{\mathrm{Re}}\tfrac{2}{3}\left(2.\frac{\partial w}{\partial z}-\frac{\partial u}{\partial x}-\frac{\partial v}{\partial y}\right),\qquad \tau_{xy}=\frac{\mu}{\mathrm{Re}}\left(\frac{\partial v}{\partial x}+\frac{\partial u}{\partial y}\right),$$

$$\tau_{yz}=\frac{\mu}{\mathrm{Re}}\left(\frac{\partial w}{\partial y}+\frac{\partial v}{\partial z}\right),\ \tau_{xz}=\frac{\mu}{\mathrm{Re}}\left(\frac{\partial u}{\partial z}+\frac{\partial w}{\partial x}\right)$$

$$k_x=\frac{1}{\mathrm{Re}}\left(\mu_l+\frac{\mu_t}{\sigma_k}\right)\frac{\partial k}{\partial x},\qquad \varepsilon_x=\frac{1}{\mathrm{Re}}\left(\mu_l+\frac{\mu_t}{\sigma_\varepsilon}\right)\frac{\partial \varepsilon}{\partial x}$$

$$k_y=\frac{1}{\mathrm{Re}}\left(\mu_l+\frac{\mu_t}{\sigma_k}\right)\frac{\partial k}{\partial y},\qquad \varepsilon_y=\frac{1}{\mathrm{Re}}\left(\mu_l+\frac{\mu_t}{\sigma_\varepsilon}\right)\frac{\partial \varepsilon}{\partial y}$$

$$k_z=\frac{1}{\mathrm{Re}}\left(\mu_l+\frac{\mu_t}{\sigma_k}\right)\frac{\partial k}{\partial z},\qquad \varepsilon_z=\frac{1}{\mathrm{Re}}\left(\mu_l+\frac{\mu_t}{\sigma_\varepsilon}\right)\frac{\partial \varepsilon}{\partial z}$$

The element of heat flux vectors are expressed by Fourier law of heat conduction as

$$q_x=\frac{k_c}{\mathrm{Re}}\frac{\partial T}{\partial x},\ q_y=\frac{k_c}{\mathrm{Re}}\frac{\partial T}{\partial y},\ q_z=\frac{k_c}{\mathrm{Re}}\frac{\partial T}{\partial z}$$

where T is the temperature and k_c is the thermal conductivity. The expression of the thermal conductivity is $k_c/k_o = c_k\ (T/T_o)^{1.5}$ where k_o is the thermal conductivity at the ambient temperature (T_o) and the value of the coefficient, c_k depends on the temperature and the ambient gas. The expression of laminar viscosity is $\mu_l/\mu_o = c_v\ (T/T_o)^{1.5}$ where μ_o is the laminar viscosity at the ambient temperature and the coefficient, c_v depends on the temperature and the ambient gas. The total viscosity $\mu=\mu_l+\mu_t$ where μ_t is the turbulent eddy viscosity and the expression of turbulent eddy viscosity, $\mu_t = c_\mu.\rho\frac{k^2}{\varepsilon}$. The Reynolds number of the flow is defined by $\mathrm{Re}=(\rho_c u_c l_c/\mu_o)$ where ρ_c, u_c, l_c and μ_o are respectively a characteristics density, a characteristics velocity, a characteristics length and the viscosity of the fluid.

The source term $S(Q)$ of the k-ε turbulence model is written by,

$$S(Q)= [0, 0, 0, 0, 0, P_k-\rho\varepsilon-D_k, (c_{\varepsilon 1}.P_k - c_{\varepsilon 2}.\rho\varepsilon)\frac{\varepsilon}{k}]$$

where the production term P_k is given in Cartesian coordinates as,

$$P_k = \{2\mu_t\frac{\partial u}{\partial x}-\tfrac{2}{3}[\rho k+\mu_t(\frac{\partial u}{\partial x}+\frac{\partial v}{\partial y}+\frac{\partial w}{\partial z})]\}\frac{\partial u}{\partial x}+$$

$$\{2\mu_t\frac{\partial v}{\partial y}-\tfrac{2}{3}[\rho k+\mu_t(\frac{\partial u}{\partial x}+\frac{\partial v}{\partial y}+\frac{\partial w}{\partial z})]\}\frac{\partial v}{\partial y}+\{2\mu_t\frac{\partial w}{\partial z}-$$

$$\tfrac{2}{3}[\rho k+\mu_t(\frac{\partial u}{\partial x}+\frac{\partial v}{\partial y}+\frac{\partial w}{\partial z})]\}\frac{\partial w}{\partial z}+\mu_t(\frac{\partial u}{\partial y}+\frac{\partial v}{\partial x})^2+$$

$$\mu_t(\frac{\partial u}{\partial z}+\frac{\partial w}{\partial x})^2+\mu_t(\frac{\partial w}{\partial y}+\frac{\partial v}{\partial z})^2 \text{ and}$$

the destruction term D_k is given as,

$$D_k=\frac{2\rho}{\gamma.T}k\varepsilon$$

The mass average turbulent kinetic energy and homogeneous component of turbulent kinetic energy dissipation rate are defined by as,

$$k=\tfrac{1}{2}.c_t^2.(u^2+v^2+w^2) \quad \text{and} \quad \varepsilon=c_m.k^2.\frac{\mathrm{Re}}{100}$$

The various constants in the k-ε turbulence model are listed as follows:
c_μ=0.09, c_t=0.03, c_m=0.09, $c_{\varepsilon 1}$=1.45, $c_{\varepsilon 2}$=1.92, σ_k=1.00, σ_ε=1.30

The following characteristics values are used for non-dimensionalized in these computations: Characteristics temperature = *298.00K,* Characteristics length = *0.0010 m,* Characteristics pressure = *101000 Pascal,* Universal Gas constant = *8.31451,* Moleculer weight = *0.029,* Ratio of specific gas constant = *1.4,* Characteristics velocity = *292.30 m/s,* Characteristics density = *1.1821 kg/m^3,* Characteristics time = *3.4 μsec,* Thermal conductivity at *0^{o}C = 0.02227 W/m-K,* Fluid viscosity at *0^{o}C = 1.603E-05 Pa.S,* Prandtl number = *0.722,* Reynolds number = *21546*

The governing equations described above for compressible viscous flow are discretised by the finite volume method. A second order, upwind Godounov scheme of Flux vector splitting method is used to discrete the inviscid flux terms and MUSCL-Hancock scheme is used for interpolation of variables. Central differencing scheme is used in discretizing the viscous flux terms. HLL Reimann solver is used for shock capturing in the flow. Two equations for k-ε turbulence model are used to determine the dissipation of turbulent kinetic energy and ε the rate of dissipation. The k and ε equations contain nonlinear production and destruction source terms, which can be very large near the solid boundaries. The upstream of incident shock wave is set as inflow boundary condition, the properties and velocities of which are calculated from Rankine-Hugoniot conditions with incident shock Mach number. The downstream inflow boundary condition and wall surface are used as solid boundary conditions where the gradients normal to the surface are taken zero. All solid walls are treated as viscous solid wall boundary. For the two-equation k-ε turbulence model on solid boundaries, μ_t is set to zero.

2.2 Grid System and Grid Adaptation

Three dimensional hexahedral cells with adaptive grids are used for these computations. In this grid system, the cell-edge data structures are arranged in such a way that each cell contains six faces which are sequence in one to six and each face indicates two neighboring cells that is left cell and right cell providing all faces of a cell are vectorized by the position and coordinate in the grid system. The initial three-dimensional grid system with turbulence-generating grids is shown in Fig.1 (i) and the two dimensional sectional view of the adaptive grids is shown in Fig.1 (ii). The physical size of each cell before adaptation is equal to 5x5x5 *(mm)*.

The grid adaptation is one of the improved and computational time saving techniques, which is used in these computations. The grid adaptation is performed by two procedures, one is refinement procedure and another is coarsening procedure. The refinement and coarsening operations are handled separately in computation. The criterion used for grid adaptation is based on the truncation error (ϵ_T) of the Taylor series expansion of density. The truncation error indicator ϵ_T is defined for every face of a cell and given by the ratio of the second-order derivative term to the first order one of the Taylor series of density so that

$$\epsilon_T = max\left[\frac{|(\nabla\rho)_{lc} - (\nabla\rho)_i|}{(\alpha_f \rho_c)/dl + |(\nabla\rho)_i|}, \frac{|(\nabla\rho)_{lc} - (\nabla\rho)_j|}{(\alpha_f \rho_c)/dl + |(\nabla\rho)_j|}\right]$$

where c represent the location of any face of a cell, i and j represent left cell and right cell of that face, dl is the center distance between cell i and j, $(\nabla\rho)_i$ and $(\nabla\rho)_j$ are the density gradient for cell i and j, $(\nabla\rho)_{lc}$= $(\rho_i$-$\rho_j)/dl$, ρ_c is the density at the interface of right cell and left cell and α_f is the constant which is initially designed to prevent a zero denominator. The value of α_f is used 0.02 and it is problem-independent parameter. The refinement and coarsening operation for any cell depends on ϵ_T

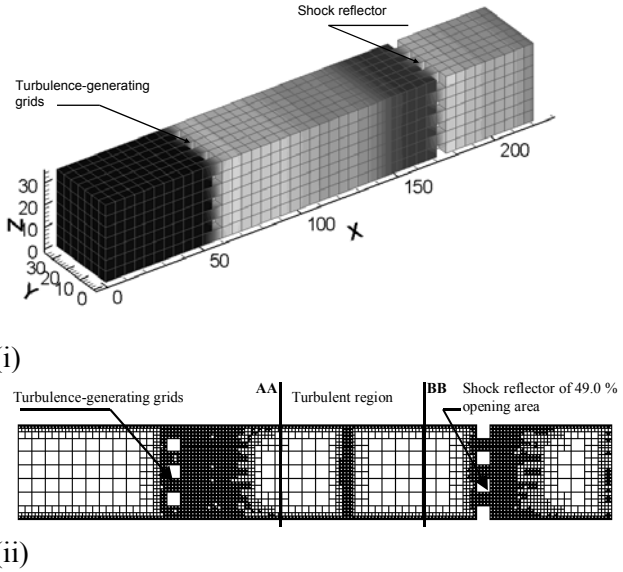

Fig.1: (i) Three dimensional grid system where the position of the turbulence generating grids and shock reflector are shown; (ii) Sectional view of adaptive ZX-plane where selected turbulent region are shown

value and the value of C_T is determined for each face of a cell. The criterion for adaptation for any cell is
Refinement = maximum C_T of six faces of a cell $>\varepsilon_r$
Coarsening = maximum C_T of six faces of a cell $<\varepsilon_c$
where ε_r and ε_c are the threshold values for refinement and coarsening. In these computations, the value of ε_r is used 0.44 and the value of ε_c is used 0.40 and the level of refinement is 3.

In the refinement procedure, the cells are selected for refinement in which every cell is divided into eight new sub cells and these new sub cells are arranged in a particular sequence so that these sub cells are used suitably in the data-structure. In the coarsening procedure, the eight sub cells, which are generated from the primary cell, are restored into the primary cell. The above three-dimensional adaptation strategy is an upgraded work of two-dimensional adaptation developed by Sun and Takayama [8].

3 Results and Discussion

In this paper, the investigation on shock reflection phenomena from different shock reflectors is focused mainly to enhance the reflected shock utilities in the shock/turbulence interaction. The incident shock utilities in the shock/turbulence interaction are the difficult task due to generation of the homogeneous turbulence field and the generation of the incident shock simultaneously. In that case, the reflected shock utilities in interaction with grid-generated shock-induced turbulence are the suitable techniques. Many researchers were used shock reflection technique from the plane end wall and they used shock-induced turbulent flow in the wake of the turbulence grid for the interaction. In the present computations, different shock reflectors of 49.0 % and 26.5 % opening area are used to get the different strengths of reflected shock wave and these results are compared with the results for the reflection from the plane end wall. In the present computations, the time-dependent Reynolds-averaged Navier-Stokes equations with k-ε turbulence model are solved by the grid adaptation technique. All the relevant parameters are resolved with k-ε turbulence model for shock Mach number, M_s = 2.00. Navier-Stokes simulation (NS) is also performed to observe the present shock reflection phenomena with the same incident shock wave. The Navier-Stokes simulation (NS) results are used to compare with the present simulation results and it is observed that there have good agreements between the present simulation results and the NS results.

After the partial reflection from different shock reflectors, different strengths of the reflected shock wave interact with the same strength of turbulence field. Shock reflector is the device and it has both the reflection and transmitting capabilities of the shock wave. Shock reflectors are classified by the open area ratio. Two types of shock reflectors are used which are shown in Fig.2 (i) and (ii). Shock reflector of 49.0 % opening area has more transmitting capabilities of the shock wave as compare to the shock reflector of 26.5 % opening area. The strength of the reflected shock wave after partial reflection from the reflector of 49.0 % opening area is comparatively weaker than the strength of the reflected shock wave after partial reflection from the reflector of 26.5 % opening area. On the other hand, the incident shock Mach number and the configuration of turbulence grid plate are same for all computations. So the strength of the shock induced turbulent flow in the wake of the turbulence grid is same for all types of computations.

To generate a compressible flow of homogeneous, isotropic turbulence, turbulence-generating grids are placed in the shock tube parallel to *YZ*-plane, which is shown in Fig.1. The total opening area of turbulence-generating grids is 51.0 *%* and the configuration of the turbulence-generating grids is shown in Fig.2 (iii). Turbulence-generating grids are uniform in size and spacing; so the shock wave and the gas flow following the shock wave after passing through turbulence-generating grids generate a compressible flow of homogeneous, isotropic turbulence. The region between the lateral plane AA and BB in Fig.1 (ii), is treated as the selected turbulent region. The centerline, along the longitudinal direction of the turbulent region is treated as the centerline of the turbulent region. 15 points of equal spacing are taken on the centerline of the turbulent region and different parameters (velocity, pressure and temperature etc.) are computed on these 15 points. The lateral planes intersect these points and parallel to the *YZ*-plane are

(i) (ii) (iii)

Fig.2: (i) The configuration of shock reflector of 49.0 % opening area (ii) The configuration of shock reflector of 26.5 % opening area (iii) The configuration of turbulence-generating grids

treated as the grid-data planes and the grids inside the turbulent region cut by the grid-data planes are the grids on the grid-data plane. The value of the turbulent parameter on the center line of the turbulent region is the average value of all the grid values of that parameter on the grid-data plane and in the present computations, the grids adjacent to the boundary are not taken into account due to viscous effect. The pressure, velocity and temperature etc, are determined across the reflected shock wave when the position of the reflected shock wave is in the turbulent region and the characteristics profiles of these parameters across the reflected shock wave are plotted to observe the reflection phenomena. The longitudinal distance (X/m) of any point on the centerline of the turbulent region are determined from the turbulence-generating girds where m = 5.0 mm, the maximum dimensional length of a grid in the grid system. The distance, X = 0.0 mm at the position of turbulence-generating grids. The value, X/m = 6.9 is the starting point of the centerline and the value, X/m = 18.2 is the ending point of the centerline of the turbulent region.

After the shock wave is diffracted through the turbulence grids, the fluid flow causes the formation of unsteady, compressible vortices and the vortices separate from the grids, then merges, dissipates and forms a compressible turbulent field at some distance downstream of the grids. It is observed that near the turbulence grids, the unsteady vorticity fluctuations in the lateral direction are high which cause more flow fluctuations in the lateral direction. The vortex fluctuations as well as vortex interaction change to fully developed turbulence field in the wake of the turbulence grids. Fig.3 shows the vorticity contour in the lateral planes at different positions along the longitudinal direction from the turbulence grids. It is observed in Fig.3 that the interaction of vortices is strong enough near the turbulence grids and the vorticity diminishes in the far distance, which indicates the change of unsteady vorticity fluctuations to homogeneous turbulence. The location where X/m>3.78, is taken as the uniform and small vorticity fluctuations region.

The average longitudinal velocity, U_{av}/c variations are determined across the reflected shock wave when the position of the reflected shock wave is in the turbulent region. The average longitudinal velocity, $U_{av} = \sum_{i=1}^{n} U_i \Big/ n$, U_i is the instantaneous velocity for any grid on the grid-data plane and n is the number of grid on the grid-data plane avoiding grids near the boundary. c is the local sound velocity. It is observed that longitudinal velocities behind the reflected shock wave are observed for the shock wave reflection from different shock reflectors of 49.0 %, 26.5 % opening area and from the plane end wall. Fig.4 shows the longitudinal velocity profiles across the reflected shock wave and a good agreement for the longitudinal velocity profiles is observed between the present simulation results and the NS results. It is observed that the longitudinal velocity behind the reflected shock wave increases and the longitudinal velocity difference across the reflected shock wave is higher for the plane end wall reflection and this difference decreases for the shock reflector of higher openings.

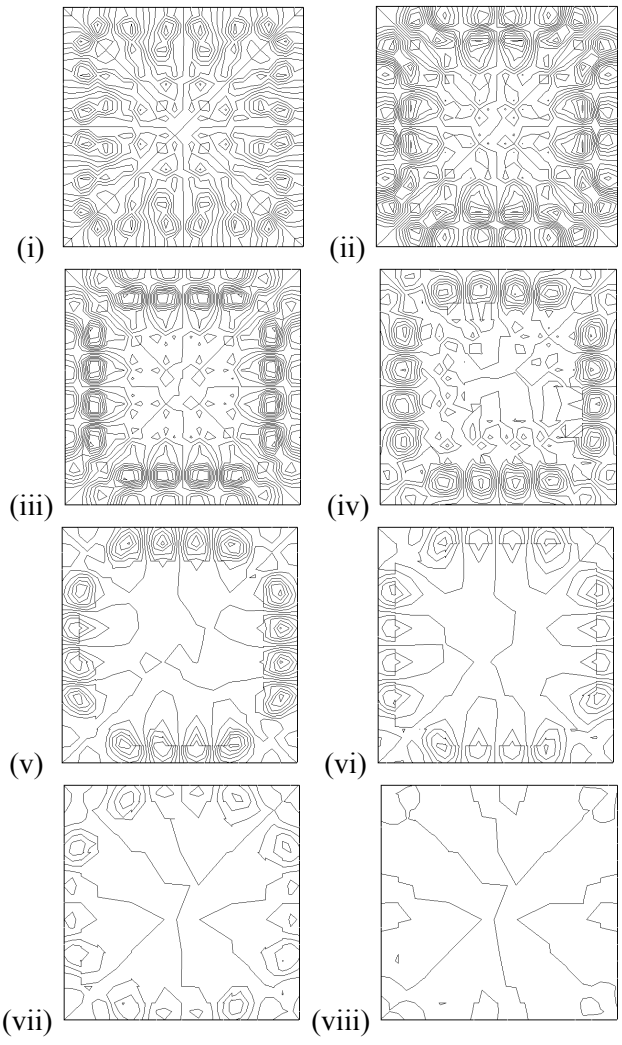

Fig.3: Vorticity contour field in the lateral plane produced by the shock diffraction at turbulence grids where the contour jump is 5.0 x 10^{-4} and minimum vorticity, maximum vorticity, lateral plane location (X/m) are (i) -50 x 10^{-4}, 50 x 10^{-4}, 0.22; (ii) -65 x 10^{-4}, 65 x 10^{-4}, 0.67; (iii) -73 x 10^{-4}, 73 x 10^{-4}, 1.22; (iv) -63 x 10^{-4}, 63 x 10^{-4}, 1.78; (v) -56 x 10^{-4}, 56 x 10^{-4}, 2.38; (vi) -41 x 10^{-4}, 41 x 10^{-4}, 2.78; (vii) -32 x 10^{-4}, 32 x 10^{-4}, 3.18; (viii) -18 x 10^{-4}, 18 x 10^{-4}, 3.78 respectively

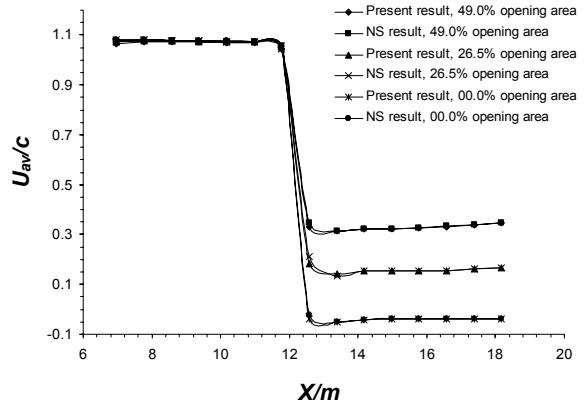

Fig.4: The longitudinal velocity profiles across the reflected shock wave for the reflection from the different shock reflectors of 49.0 %, 26.5 % opening area and the plane end wall

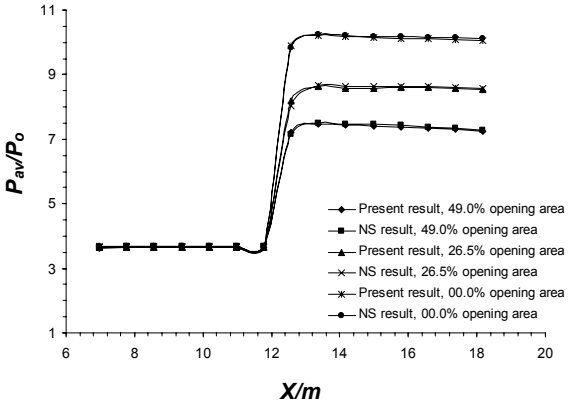

Fig.5: The average pressure profiles across the reflected shock wave for the reflection from different shock reflectors of 49.0 %, 26.5 % opening area and the plane end wall

The normalized pressure, P_{av}/P_o variations are determined across the reflected shock wave when the position of the reflected shock wave is in the turbulent region where the average pressure, $P_{av} = \sum_{i=1}^{n} P_i \Big/ n$, P_i is the instantaneous pressure for any grid on the grid-data plane and n is the number of grid on the grid-data plane avoiding grids near the boundary. P_o is the STD atmospheric pressure. Fig.5 shows the pressure profiles across the reflected shock wave for the shock wave reflection from different shock reflectors and the pressure profiles obey the shock reflection theory. The average pressure difference between downstream and upstream of the reflected shock wave depends on the opening area of the shock reflector and the pressure profiles across the reflected shock wave have the good agreement with the NS results. The strength of the reflected shock wave is decreased for the reflection from the shock reflector of higher opening area and the strength is increased as increasing the blockage ratio of the reflector. The maximum strength of the reflected shock wave is obtained for the reflection from the plane end wall. After measuring the transmitted shock Mach number, it is shown that the value of transmitted shock Mach number is 1.83 for the incident shock Mach number, M_s = 2.00. Table-1 shows the value of transmitted shock Mach number and the partial reflected shock Mach number for the incident shock Mach number, M_s = 2.00.

Table 1

Type of shock reflector	Incident shock Mach number	Transmitted shock Mach number after turbulence grid	Reflected shock Mach number after reflection from shock reflector
49.0 % opening area	2.00	1.83	1.66
26.5 % opening area	2.00	1.83	1.73
Plane end wall	2.00	1.83	1.90

The total temperature (T/T_o) variations are determined across the reflected shock wave for the different shock reflection techniques, which are shown in Fig.6. It is observed that the temperature variations are occurred in the interaction region and the higher temperature variations at different points in the interaction region are observed for the strong reflected shock wave. It is also observed that the measurements of the temperature variations by the present computational techniques have the good agreements with the NS results.

The dissipative-length scale is defined by the expression, $k^{3/2}/\varepsilon$ where the turbulent kinetic energy, $k = \sum_{i=1}^{n} k_i \Big/ n$ and k_i is the instantaneous turbulent kinetic energy for any grid on the grid-data plane and n is the number of grid on the grid-data plane where the grids adjacent to the boundary are not taken into account due to viscous effect. Similarly the dissipation rate, $\varepsilon = \sum_{i=1}^{n} \varepsilon_i \Big/ n$ where ε_i is the instantaneous turbulent kinetic energy dissipation rate for any grid on the grid-data plane. The

amplification of dissipative-length scale is the ratio of the dissipative-length scale after interaction to the dissipative-length scale before interaction. The amplification of dissipative-length scale is determined along the centerline of the turbulent region in the interaction of different strengths of reflected shock wave with similar flow fields and the characteristics profiles of the amplification of dissipative length scale are plotted along the centerline of the turbulent region for the reflection from different shock reflectors, which is shown in Fig.7. It is observed that the amplification of dissipative-length scale decreases in all the cases of shock/turbulence interaction. The DNS data of Lee, Lele and Moin [9] and the DNS data of Hannappel and Friedrich [10] indicate that the velocity length scale and the dissipative-length scale decrease through shock interaction. The dissipative-length scale in the experiment of Honkan and Andreopoulos [1] was found to increase after the interaction. The DNS results of Lee, Lele and Moin [11] have indicated a small increase of dissipative-length scales through weak shock interactions. The length scale is reduced for stronger shock waves, while it shows a mild increase for shock waves with shock Mach number less than 1.65. In the present computations, the amplification of dissipative-length scale is decreased after the interaction of strong shock wave with turbulence. Due to stronger compressibility effects, the amplification of dissipative-length scale decreases more in the interaction of stronger shock wave with turbulence.

The velocity length scale is defined by the expression, $k^{1/2}$. The amplification of velocity length scale is the ratio of the velocity length scale after interaction to the velocity length scale before interaction. The amplification of velocity length scale is determined along the centerline of the turbulent region in the interaction of different strengths of reflected shock wave with similar flow fields and the characteristics profiles of the amplification of velocity length scale are plotted along the centerline of the turbulent region for the reflection from different shock reflectors, which is shown in Fig.8. It is observed that the amplification of velocity length scale decreases in the interaction of strong shock wave with turbulence.

The rate of dissipation of turbulent kinetic energy (TKE), ε is determined before and after the interaction of different strengths of shock wave with the similar turbulent fields. Fig.9 shows the profiles for the variations of TKE dissipation rate along the centerline of the turbulent region. It is observed that in all cases, the TKE dissipation rate decreases after

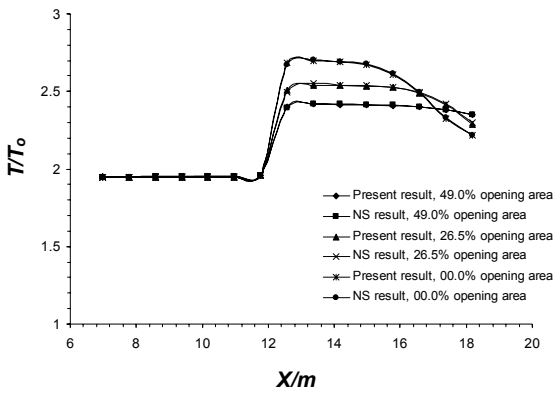

Fig.6: The total temperature profiles across the reflected shock wave for the reflection from the different shock reflectors of 49.0 %, 26.5 % opening area and the plane end wall

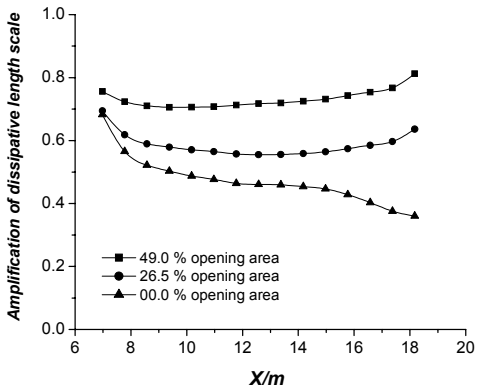

Fig.7: The amplification of dissipation length scale profiles along the centerline of the turbulent region for the reflection from the different shock reflectors

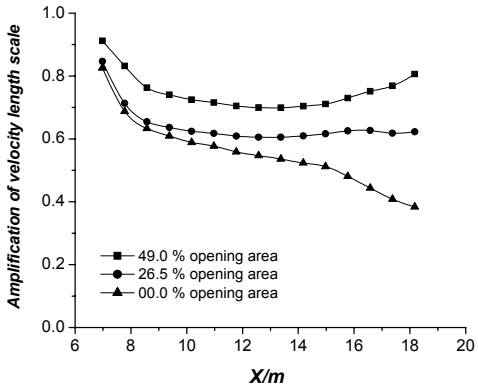

Fig.8: The amplification of velocity length scale profiles along the centerline of the turbulent region for the reflection from the different shock reflectors

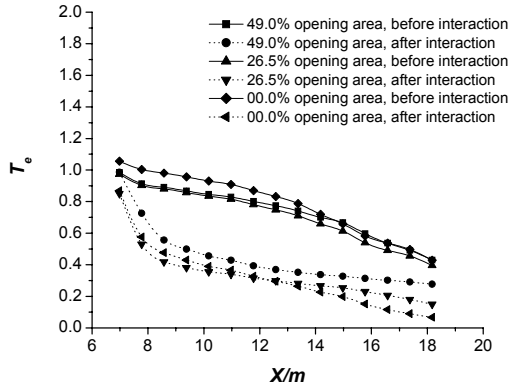

Fig.9: Dissipation rate of TKE, T_e (where $T_e = 10^5\varepsilon$) before and after the shock/turbulence interaction for the reflection from the different shock reflectors of 49.0 %, 26.5 % opening area and the plane end wall

the shock/turbulence interaction and the higher value of dissipation rate is observed in the interaction of comparatively stronger shock wave with turbulent flow. Many researchers got the same results about the decreasing of the dissipation rate after the interaction.

4 Conclusion

The reflection of the shock wave from different shock reflectors has been investigated by means of Navier-stokes simulations with turbulence model. The results have been compared with the NS results. The simulation results show that the longitudinal velocity behind the reflected shock wave increases due to partial reflection from the shock reflectors and it is possible to find out the outcomes of the interaction of different strengths of shock wave with turbulence. The different strengths of the shock waves after the reflection from the shock reflectors enter in the similar turbulent regions. The outcomes of shock/turbulence interaction strongly depend on the reflection techniques. Even though it is very difficult to locate the starting point of the homogeneous turbulence region but the vorticity contour at different points on the center line of the shock tube can give the preliminary ideas on the homogeneous turbulence region. In the case of full reflection, the temperature deviations in the downstream of the reflected shock wave are higher as compare to the temperature deviations in the case of partial reflection. The amplification of dissipative length scale decreases after the shock/turbulence interaction and more decreasing values are observed for the reflection from the plane end wall. Similarly the amplification of velocity length scale also decreases and more decreasing values are observed for the reflection from the plane end wall. After the shock/turbulence interaction, it is observed that the rate of dissipation is decreased and the higher values of dissipation rate are observed in the interaction of the stronger shock wave with the turbulent flow.

References:

[1] Honkan A, Andreopoulos J, "Rapid compression of grid-generated turbulence by a moving shock wave." *Phys.Fluids,* Vol. **A4**, 1992, pp. 2562-72.

[2] Keller J, Merzkirch W, "Interaction of a normal shock wave with a compressible turbulent flow." *Experiments in Fluids*, **Vol. 8**, 1990, pp. 241-248.

[3] Devieve JF, Lacharme JP, "A shock wave/free turbulence interaction." *Turbulent shear layer/shock wave interaction*, edited by J. Delery, Springer-Verlag, Berlin, 1986.

[4] Jacquin L, Blin E, Geffroy P, "Experiments of free turbulence/shock wave interaction. Proc. Turbulent shear flows, 8, tech Univ, Munich, Ger. pp 1-2-1-1-2-6, 1991.

[5] Hesselink L, Sturtevant, " Propagation of weak shocks through a random medium." *J. Fluid Mechanics,* **Vol. 196**, 1988, pp. 513-53.

[6] Rotman D. "Shock wave effects on a turbulent flows." *Phys. Fluids* **A, Vol. 3, No. 7,** 1991, pp. 1792-806.

[7] Lee S, Lele SK, Moin P, "Direct numerical simulation and analysis of shock turbulence interaction." *AIAA* paper, 91-0523, 1991a.

[8] Sun, M. and Takayama, K, "Conservative smoothing on an adaptive quadrilateral grid." *Journal of Computational Physics,* **Vol. 150,** 1999, pp. 143-180.

[9] Lee S, Lele SK, Moin P. "Direct numerical simulation of isotropic turbulence interacting with a weak shock wave." *Journal of Fluid Mechanics,* **Vol. 251,** 1993, pp. 533-62.

[10] Hannappel R, Friedrich R, "Direct numerical simulation of a Mach 2 shock interacting with isotropic turbulence." Appl. Sci. res., **Vol. 54**, 1995, pp. 205-21.

[11] Lee S, Lele SK, Moin P, "Interaction of isotropic turbulence with a strong shock wave." AIAA paper 94-0311, Dept. Mech. Eng., Stanford Univ., CA, 1994.